


Spin-based continuous Bayesian magnetic-field estimations aided by feedback control

Ethan Turner,^{*} Shu-Hao Wu[✉],^{*} Xinzhu Li, and Hailin Wang[✉]
Department of Physics, University of Oregon, Eugene, Oregon 97403, USA

 (Received 25 July 2022; accepted 20 October 2022; published 7 November 2022)

We demonstrate continuous real-time Bayesian estimations of magnetic-field fluctuations by monitoring single-photon emissions from a diamond nitrogen vacancy center under the setting of coherent population trapping, for which the time sequence of the single-photon emissions is correlated with the underlying magnetic-field fluctuations. The Bayesian estimations are combined with a feedback loop and are followed by a separate verification and optimization process, which uses the spin-dephasing rate in the presence of the feedback as a cost function. The dephasing rate is measured with Ramsey interferometry and is minimized by systematically varying the statistical parameters used in the estimations. The Bayesian estimations aided by the feedback and verification enable continuous real-time sensing at the single-photon level regardless of the prior availability of the statistical parameters of the underlying dynamics.

DOI: [10.1103/PhysRevA.106.052603](https://doi.org/10.1103/PhysRevA.106.052603)

I. INTRODUCTION

Spin-based quantum sensors, such as single nitrogen vacancy (NV) centers in diamond, allow sensitive measurements of magnetic- and electric fields, temperature, and strain with nanometer spatial resolution [1–6]. Although nearly all quantum sensors of single spins have been based on transient Ramsey interferometry, which consists of three sequential steps: initialization, coherent time evolution, and readout of the single spin [7], quantum sensing can in principle take place by continuously monitoring the sensor through photon counting, as proposed in recent theoretical studies [8–13]. Bayesian parameter estimations (BPE) have also played a major role in the development of quantum sensors. Incorporating BPE in Ramsey interferometry has led to major improvements in measurement sensitivity, dynamic range, and speed [14–19]. For the continuous quantum sensing, BPE can update the estimation in real time with the detection of just a single photon, as shown in recent studies [13,20]. However, these studies have also revealed that the continuous updating at the single-photon level can provide dynamical information, only if the statistical properties of the underlying dynamical fluctuations are already known and are taken advantage of in the BPE. This requirement is difficult to fulfill for many intended applications.

In this paper, we report the experimental demonstration of spin-based continuous BPE that combine the conventional BPE with a feedback loop [21], followed by a separate verification and optimization process. For the feedback, we apply an additional magnetic field to the NV center to cancel the estimated magnetic-field variation. We then verify possible feedback-induced suppression of spin dephasing by using Ramsey interferometry. A key aspect of our approach is to use the spin-dephasing rate in the presence of the feedback

as an effective cost function for the BPE. We can minimize the cost function and thereby optimize the BPE by systematically varying the statistical parameters used in the BPE. This verification and optimization process provides us valuable information on the essential statistical properties of the underlying dynamics. Furthermore, initial cycles of verification and optimization enable the later continuous BPE that can update dynamical information in real time with the detection of a single photon regardless of the prior availability of the statistical parameters of the underlying dynamics. The continuous BPE aided by feedback thus successfully overcomes the key obstacle encountered in the earlier approach of continuous BPE, adding a powerful tool to the quantum sensing toolkit and opening another frontier for exploring quantum dynamics, quantum fluctuations, and feedback control at the nanoscale [22,23].

II. EXPERIMENT METHODS

We carry out the continuous real-time magnetic-field sensing under the setting of coherent population trapping (CPT), for which the $m_s = 0$ and $m_s = +1$ ground spin states of a NV center, with a frequency separation ω_B , are coupled to the E_y excited state with two respective resonant laser fields (see Fig. 1) [24–26]. CPT due to destructive quantum interference occurs when the optical coupling is Raman resonant, i.e., when $\delta - \omega_B = 0$, where δ is the detuning between the two laser fields. As illustrated in Fig. 1, when the average Raman detuning (i.e., the Raman bias), $\Delta = \delta - \langle \omega_B \rangle$, is near the half-width of the CPT spectral response, single-photon emissions from the NV center are directly correlated with the magnetic-field variations, provided that the variations in ω_B do not exceed the half-width. Specifically, $\{\mathbf{y}_n\} = \{y_1, y_2, \dots, y_n, \dots\}$, where y_n is the number of photons detected during the n th time interval with equal duration τ , carries the information on $\{\mathbf{x}_n\} = \{x_1, x_2, \dots, x_n, \dots\}$, the corresponding change in ω_B .

^{*}These authors contributed equally to this work.

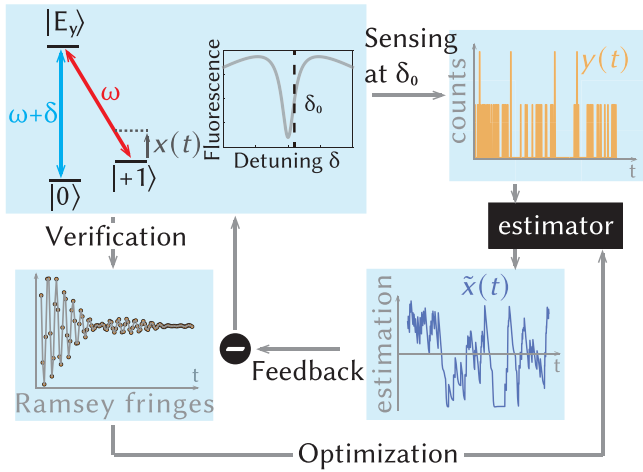


FIG. 1. Schematic of continuous quantum sensing via CPT and with feedback control. Upper-left figure shows the Λ -type three-level system used for the CPT process. With the laser detuning fixed near the half-width of the spectral CPT response, a Bayesian estimator can convert in real time the time series of detected single-photon emissions into changes in the frequency separation between the two ground spin states. For the feedback, an additional magnetic field is applied to the NV center to cancel the estimated change. The feedback-induced reduction in the NV spin-dephasing rate is verified with Ramsey interferometry.

We use Bayesian inference and the time series of the detected photon counts, $\{y_n\}$, to generate a time series of estimated frequency changes, $\{\tilde{x}_n\} = \{\tilde{x}_1, \tilde{x}_2, \dots, \tilde{x}_n, \dots\}$. For the Bayes update,

$$p(x_n|y_n, y_{n-1}, \dots, y_1) \propto p_{\bar{y}_n}(y_n|x_n) \times p'(x_n|y_{n-1}, \dots, y_1), \quad (1)$$

where $p'(x_n|y_{n-1}, \dots, y_1)$ is the prior probability distribution, $p(x_n|y_n, y_{n-1}, \dots, y_1)$ is the posterior probability distribution, and $p_{\bar{y}_n}(y_n|x_n)$ is the likelihood of detecting y_n photons in the n th time interval given x_n and follows a Poisson distribution,

$$p_{\bar{y}_n}(y_n|x_n) = \frac{\bar{y}_n^{y_n} e^{-\bar{y}_n}}{y_n!}, \quad (2)$$

with \bar{y}_n being the expected average photon count per updating time interval. The estimation is then given by

$$\tilde{x}(t) = \int p(x, t) x dx. \quad (3)$$

To achieve good time resolution for the real-time sensing, we have $\bar{y}_n \ll 1$. Under this condition, Bayesian estimations with a prior that is simply given by the previous estimate quickly converge to the average value of $x(t)$ and provide no information on the dynamics of $x(t)$, as shown in earlier studies [13,20].

The dynamical information can be obtained with an improved prior, which takes into consideration the statistical properties of $x(t)$. Many dynamical processes of interest can be modeled as an Ornstein-Uhlenbeck (OU) process [12,27,28], which is a stationary Gauss-Markov process and features an autocorrelation function,

$$R(t) = \langle x(t_0)x(t_0 + t) \rangle = \sigma^2 e^{-|t|/\tau_c}, \quad (4)$$

with σ^2 and τ_c being the variance and the correlation time, respectively. For these OU processes, we take the improved prior as

$$\begin{aligned} p'(x_n = x|y_{n-1}, \dots, y_1) &= \int d\omega p(x_{n-1}) \\ &= x - \omega|y_{n-1}, \dots, y_1) \\ p_{\text{OU}}(x_n = x_{n-1} + \omega, t + \tau|x_{n-1}, t), \end{aligned} \quad (5)$$

where p_{OU} is the probability of finding x_n at $t + \tau$ given x_{n-1} at t for the OU process,

$$\begin{aligned} p_{\text{OU}}(x_n, t + \tau|x_{n-1}, t) \\ = \mathbb{N}(x_{n-1} e^{-\tau/\tau_N}, \sigma^2 [1 - \exp(-2\tau/\tau_N)]), \end{aligned} \quad (6)$$

with \mathbb{N} denoting a normal distribution [13]. We refer to this Bayesian estimator as the OU-Bayesian estimator.

For a proof-of-principle experimental demonstration, we apply to the NV center an external magnetic-field fluctuation that follows an OU process with $\langle x(t) \rangle = 0$. Note that the use of the improved prior requires that the statistical parameters of the OU process be already known before the sensing process. To combine the continuous sensing process with a feedback loop, we apply to the NV center an additional magnetic field to effectively subtract the estimated magnetic field from the external fluctuations. The feedback-induced reduction in the NV spin-dephasing rate can be measured with a Ramsey interferometry experiment that immediately follows the sensing cycle. We can optimize the Bayesian estimator by varying the statistical parameters used in the BPE and by minimizing the spin-dephasing rate, as illustrated schematically in Fig. 1.

For the experimental implementation, an electronic-grade chemical-vapor deposition grown diamond sample (from Element Six, Inc.) was cooled down to 10 K in an optical cryostat from Montana Instruments, Inc. Optical excitation and collection were carried out with a confocal optical microscope and with a solid immersion lens (SIL) milled into the surface of the diamond. A permanent magnet placed outside of the cryostat was used to split the $m_s = \pm 1$ states by 430 MHz. For the two optical fields used in CPT, a tunable 637-nm diode laser was tuned to the $m_s = +1$ to E_y transition while a sideband generated by an electro-optical modulator was tuned to the $m_s = 0$ to E_y transition. The CPT spectral response used for the continuous sensing has a linewidth of 17.9 MHz, including contributions from the hyperfine splitting (2.2 MHz), spin dephasing (0.62 MHz), and power broadening with an estimated Rabi frequency of 10.6 MHz. A schematic of the experimental setup as well as a CPT spectral response is presented in the Supplemental Material in an earlier study [20].

The external time-varying magnetic field was applied to the NV center through a coplanar waveguide (CPW) fabricated next to the SIL. The current through the CPW, which follows a simulated OU process, was generated by an arbitrary function generator (AFG). Microwave (MW) pulses used for Ramsey interferometry were also applied via the CPW, with Rabi frequency, $\Omega_{\text{MW}}/2\pi = 20$ MHz, and were detuned from the $m_s = 0$ to $m_s = +1$ transition by $\delta_{\text{MW}}/2\pi = 60$ MHz. For feedback control, an additional magnetic field needs to be applied to the NV center to cancel the estimated change in the

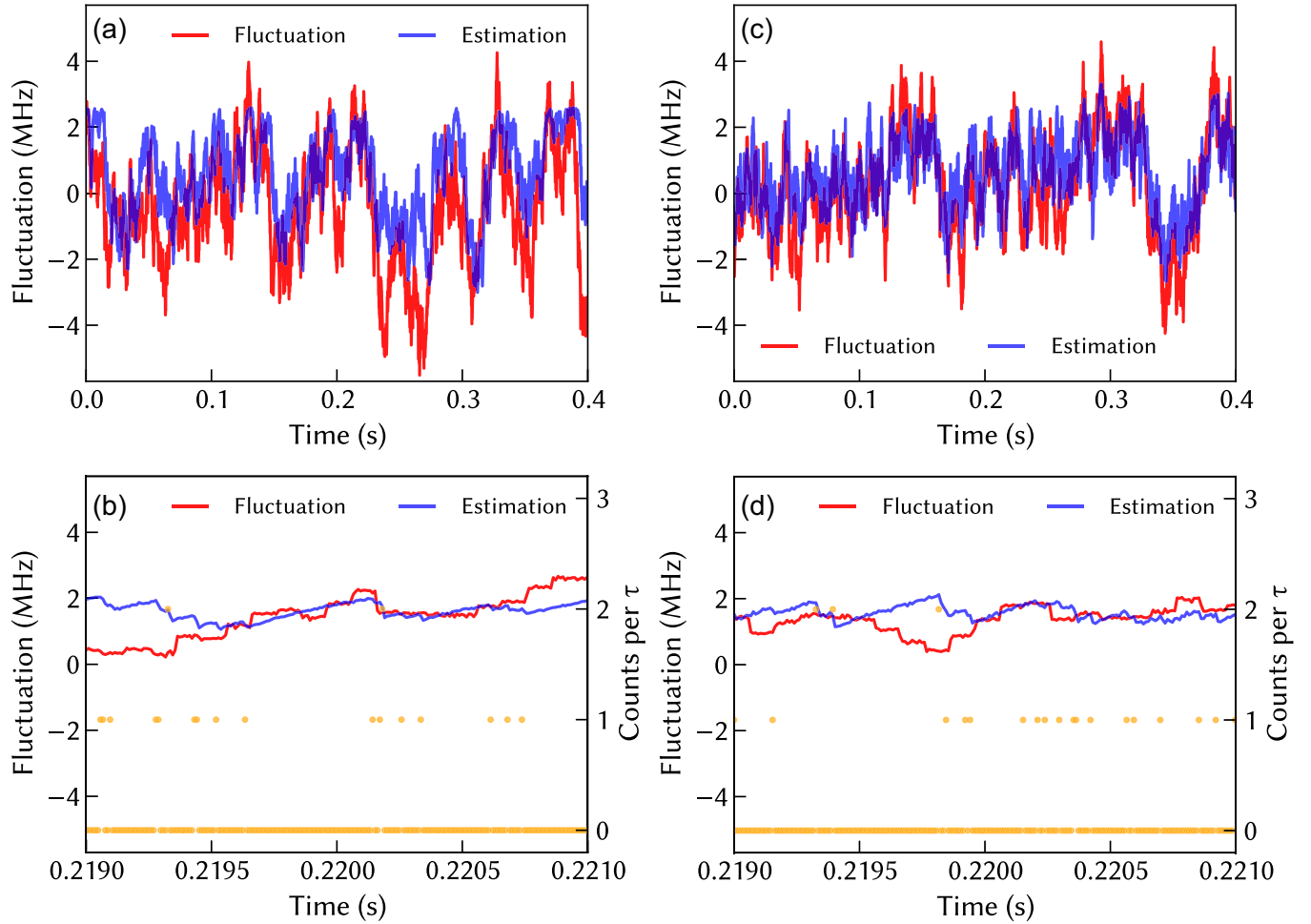


FIG. 2. (a), (b) Continuous real-time estimations of $x(t)$ obtained without feedback. (c), (d) Estimations of $x(t)$ obtained with feedback. The red curves are the actual OU-type fluctuations and the blue curves are the corresponding estimations. The orange dots in (b) and (d) show the photon counts per updating time interval, τ , which is set to $10 \mu\text{s}$. The correlation between the sawtooth behavior in the estimations and the detection of a single photon demonstrates the updating of dynamical information with the detection of a single photon. Statistical parameters used for the external OU fluctuations are $\tau_c = 10 \text{ ms}$ and $\sigma/2\pi = 1.9 \text{ MHz}$.

magnetic field from the OU external magnetic field. Experimentally, this was implemented through the subtraction of the corresponding voltage in the output of the AFG. For BPE, this additional magnetic field can be treated as an effective shift in $\langle\omega_B\rangle$.

For the continuous BPE, the experiment began with the initialization of the NV to the $m_s = 0$ state using a $10\text{-}\mu\text{s}$ green laser pulse ($\lambda = 532 \text{ nm}$), followed by two long ($100\text{-}\mu\text{s}$) optical pulses that induce CPT. The fluorescence was continuously collected during the CPT process. Unless otherwise specified, the Raman bias used is $(\delta_0 - \langle\omega_B\rangle)/2\pi = 3 \text{ MHz}$ and the average photon count rate is near $13000/\text{s}$. BPE were carried out with a field-programmable gate array (FPGA) in a Keysight M3302A card containing a digitizer and an arbitrary waveform generator, which accumulates the number of photon counts per update time interval and outputs a voltage corresponding to the estimated frequency fluctuations. The technical details of implementing the continuous BPE are discussed in the Supplemental Material in an earlier study [20].

III. EXPERIMENT RESULTS

A. Continuous Bayesian parameter estimations

Figure 2(a) shows, as an example, estimations, i.e., \tilde{x}_n , obtained with the OU-Bayesian estimator without the feedback, as well as the actual fluctuations, x_n . Figure 2(b) compares the estimations obtained in a relative short time span with the corresponding time series of the detected photon counts. Since $\bar{y}_n \ll 1$, the estimator waits for the arrival of a detected photon to output an estimation, leading to the sawtooth behavior shown in Fig. 2(b). The correlations between the sawtooths and the photon counts in Fig. 2(b) demonstrate that the continuous real-time estimation effectively updates the dynamical information with the detection of just a single photon. For comparison, it took about 100 detected photons to obtain an estimation in an earlier study that uses the complete CPT spectrum of a single NV to probe the magnetic fluctuations induced by the nuclear spin bath [29].

Figure 2(c) shows estimations obtained under the same conditions as those for Fig. 2(a) except that now the

estimations are carried out with the feedback loop, which subtracts estimated change, \tilde{x}_{n-1} , from x_n such that the actual net change in ω_B is $x_n - \tilde{x}_{n-1}$. In this case, the OU-Bayesian estimations take place with a shifted Raman bias, $\delta - (\langle\omega_B\rangle - \tilde{x}_{n-1})$. Note that Figs. 2(c) and 2(d) display the estimations for x_n , not $x_n - \tilde{x}_{n-1}$. Similar to Fig. 2(b), Fig. 2(d) shows that the continuous estimation with the feedback loop updates the dynamical information with the detection of just a single photon. Note that while there is only a slight improvement in the estimations obtained with feedback control, the primary purpose in adding the feedback control is to be able to carry out OU-Bayesian estimations even when the statistical parameters of the magnetic fluctuations are initially unavailable and to verify the result of the real-time estimations, as will be discussed below.

B. Verification and optimization

The external time-varying magnetic field applied to the NV center leads to extra spin dephasing, even though τ_c is long compared with spin-dephasing time, T_2^* . The extra dephasing arises from the variations of the external field in different measurement cycles. With the feedback loop, a reduction in the magnetic-field fluctuations suppresses the extra spin dephasing. We can use this suppression of the extra spin dephasing, as determined from a Ramsey interferometry measurement, as a verification that the estimation approaches the actual change.

The pulse sequence used for the verification is shown in Fig. 3(a). After each 100- μ s-long sensing interval, verification of the feedback process was carried out by Ramsey interferometry. Each Ramsey measurement started with a 10- μ s green initialization pulse, followed by a MW $\pi/2$ pulse, which places the NV center in a superposition between the $m_s = 0$ and $m_s = +1$ spin states. The NV center was then allowed to freely precess for a variable duration, τ_{Ramsey} . After applying a second MW $\pi/2$ pulse, the electron population in the $m_s = 0$ spin state was read out through the $m_s = 0$ to E_y transition.

Figure 3(b) compares the results of the Ramsey interferometry obtained with and without the feedback loop. We numerically fit the Ramsey fringes with the sum of three sine functions (with $m_l = 0, +1, -1$), multiplied by a Gaussian envelope, $\exp[-(t/T_2^*)^2]$. A spin-dephasing time, T_2^* , of 182 and 90 ns is derived from the least-square fit of the experimental results obtained with and without the feedback loop, respectively.

The feedback and verification discussed above give us an effective mechanism to obtain information on the statistical parameters of the underlying dynamical process. In this case, we can repeat the feedback and verification cycles shown in Fig. 3(a), while systematically varying the two statistical parameters, σ and τ_c , used in the OU-Bayesian estimator. Figure 4(a) plots the heat map of T_2^* obtained from the Ramsey interferometry as a function of σ and τ_c used for the BPE. In this case, $1/T_2^*$ effectively serves as a cost function for the BPE, i.e., the smaller $1/T_2^*$ is, the smaller the estimation error becomes. The maximum improvement of T_2^* by feedback control is plotted in Fig. 4(b)

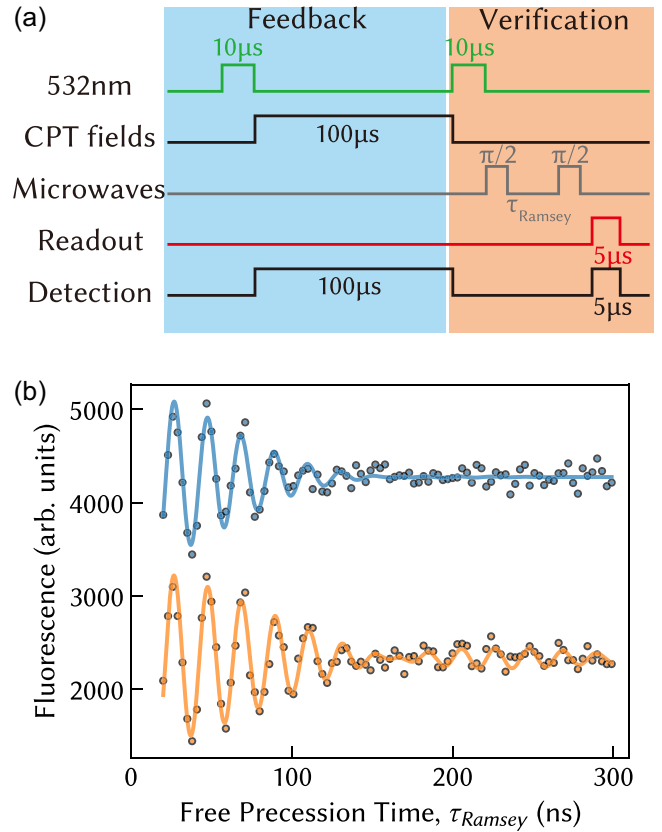


FIG. 3. (a) Pulse sequence used for the Ramsey interferometry following a cycle of BPE in the presence of feedback. The spin readout takes place via the $m_s = 0$ to E_y transition. (b) Results of Ramsey interferometry obtained with (bottom curve) and without (top curve, offset in y axis for clarity) feedback control. Statistical parameters used for the external OU fluctuations are $\tau_c = 15$ ms and $\sigma/2\pi = 2.2$ MHz. The feedback leads to an effective reduction in the overall spin-dephasing rate. The solid curves show the least-square numerical fit discussed in the text.

as a function of the memory time of the external magnetic fluctuations.

As shown in Fig. 4(a), the maximum T_2^* occurs when τ_c used for the BPE is the same as the corresponding parameter for the actual fluctuations. The repeated cycles of feedback and verification thus correctly optimized parameter τ_c . In comparison, there is a slight deviation between the optimized σ and the corresponding expected value, as can be seen from the heat map in Fig. 4(a). This deviation is in large part due to experimental uncertainties in the estimation process. In addition, the optimal sensing, i.e., the Cramer-Row lower bound, for the estimation process can be achieved only if the relevant CPT spectral response is either linear or quadratic, which is not the case for the experiment.

The improvement of T_2^* by feedback control shown in Fig. 4(b) is relatively modest. This is in part because the estimation process is relatively slow. Even with updating at the single-photon level, the average time between updates is still about 77 μ s, the inverse of the photon count rate. Both the estimations and the feedback control are thus more effective with relatively slow fluctuations. Figure 4(b) shows that the

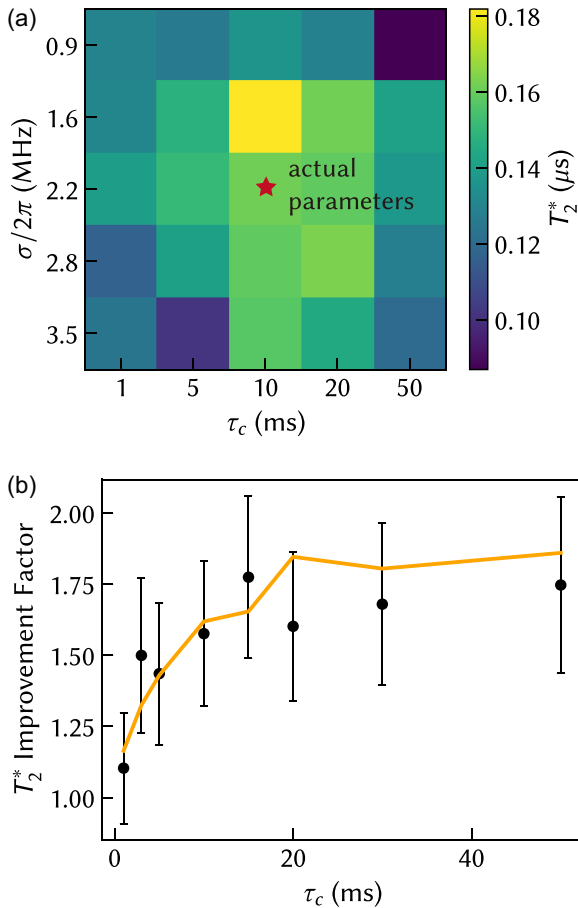


FIG. 4. (a) Spin-dephasing time, T_2^* , with feedback loop derived from Ramsey interferometry and plotted as a function of the memory time and the standard deviation used in the BPE. Actual statistical parameters are $\tau_c = 10$ ms and $\sigma/2\pi = 2.2$ MHz. Maximum T_2^* obtained under feedback loop occurs at $\tau_c = 10$ ms and $\sigma/2\pi = 1.6$ MHz. (b) Maximum improvement in T_2^* due to feedback control observed as a function of the memory time of the external magnetic-field fluctuations. Error bars in (b) are derived from the least-square numerical fit. Solid orange line is the improvement in T_2^* obtained in a numerical simulation based on the experimental parameters.

improvement observed increases with increasing τ_c for the OU fluctuations, though the improvement starts to saturate

when τ_c exceeds 10 ms. At the relatively long τ_c , the improvement becomes limited by the accuracy of the estimations. The improvement will ultimately be limited by the Cramer-Rao lower bound of the estimation process. Overall, the experimentally observed improvement is in good agreement with that obtained from the corresponding numerical simulation, as shown in Fig. 4(b), for which the experimental parameters, including the experimentally obtained average CPT spectral response, were used. The simulation of the BPE followed the same approach as that used in the earlier study [13]. The finite dynamical range of the FPGA was also accounted for in the simulation. It should be noted that the modest improvement in T_2^* does not affect the optimization of the statistical parameters used for the BPE, though greater improvement in T_2^* can lead to more robust optimization.

IV. CONCLUSION

By combining continuous BPE with feedback and verification, we have demonstrated continuous Bayesian magnetic-field sensing in real time at the single-photon level under the setting of CPT in a diamond NV center. Other spin systems that feature similar CPT processes can also be used for the continuous quantum sensing. The BPE used in this work assume that the dynamical process involved is an OU process, which is applicable to a wide variety of dynamical phenomena such as nuclear spin fluctuations [27,28]. The BPE can also be extended to other types of dynamical processes, such as random telegraph noise [30]. In cases where the statistical model is unknown, machine-learning techniques such as neural networks can be used for the estimations. In all these cases, the spin-dephasing rate in the presence of feedback can be used as an effective cost function for the verification and optimization of the relevant estimation process.

Finally, we note that CPT-based magnetometry using a NV center is limited to applications at low temperature. Potential room-temperature applications will likely require the development of color centers (in diamond or other host materials) that can feature both spectrally sharp optical absorption resonance and robust spin coherence at room temperature.

ACKNOWLEDGMENT

This work has been supported by the US ARO MURI Grant No. W911NF-18-1-0218.

- [1] J. M. Taylor, P. Cappellaro, L. Childress, L. Jiang, D. Budker, P. R. Hemmer, A. Yacoby, R. Walsworth, and M. D. Lukin, High-sensitivity diamond magnetometer with nanoscale resolution, *Nat. Phys.* **4**, 810 (2008).
- [2] J. R. Maze, P. L. Stanwix, J. S. Hodges, S. Hong, J. M. Taylor, P. Cappellaro, L. Jiang, M. V. G. Dutt, E. Togan, A. S. Zibrov, A. Yacoby, R. L. Walsworth, and M. D. Lukin, Nanoscale magnetic sensing with an individual electronic spin in diamond, *Nature (London)* **455**, 644 (2008).
- [3] G. Balasubramanian, I. Y. Chan, R. Kolesov, M. Al-Hmoud, J. Tisler, C. Shin, C. Kim, A. Wojcik, P. R. Hemmer, A. Krueger, T. Hanke, A. Leitenstorfer, R. Bratschitsch, F. Jelezko, and

J. Wrachtrup, Nanoscale imaging magnetometry with diamond spins under ambient conditions, *Nature (London)* **455**, 648 (2008).

- [4] F. Dolde, H. Fedder, M. W. Doherty, T. Nobauer, F. Remp, G. Balasubramanian, T. Wolf, F. Reinhard, L. C. L. Hollenberg, F. Jelezko, and J. Wrachtrup, Electric-field sensing using single diamond spins, *Nat. Phys.* **7**, 459 (2011).
- [5] G. Kucsko, P. C. Maurer, N. Y. Yao, M. Kubo, H. J. Noh, P. K. Lo, H. Park, and M. D. Lukin, Nanometre-scale thermometry in a living cell, *Nature (London)* **500**, 54 (2013).
- [6] M. W. Doherty, V. V. Struzhkin, D. A. Simpson, L. P. McGuinness, Y. F. Meng, A. Stacey, T. J. Karle, R. J. Hemley,

- N. B. Manson, L. C. L. Hollenberg, and S. Prawer, Electronic Properties and Metrology Applications of the Diamond NV-Center Under Pressure, *Phys. Rev. Lett.* **112**, 047601 (2014).
- [7] C. L. Degen, F. Reinhard, and P. Cappellaro, Quantum sensing, *Rev. Mod. Phys.* **89**, 035002 (2017).
- [8] A. H. Kiilerich and K. Molmer, Estimation of atomic interaction parameters by photon counting, *Phys. Rev. A* **89**, 052110 (2014).
- [9] S. Gammelmark and K. Molmer, Fisher Information and the Quantum Cramer-Rao Sensitivity Limit of Continuous Measurements, *Phys. Rev. Lett.* **112**, 170401 (2014).
- [10] A. H. Kiilerich and K. Molmer, Parameter estimation by multi-channel photon counting, *Phys. Rev. A* **91**, 012119 (2015).
- [11] L. Cortez, A. Chantasri, L. P. Garcia-Pintos, J. Dressel, and A. N. Jordan, Rapid estimation of drifting parameters in continuously measured quantum systems, *Phys. Rev. A* **95**, 012314 (2017).
- [12] C. Zhang and K. Molmer, Estimating a fluctuating magnetic field with a continuously monitored atomic ensemble, *Phys. Rev. A* **102**, 063716 (2020).
- [13] S. H. Wu, E. Turner, and H. L. Wang, Continuous real-time sensing with a nitrogen-vacancy center via coherent population trapping, *Phys. Rev. A* **103**, 042607 (2021).
- [14] R. S. Said, D. W. Berry, and J. Twamley, Nanoscale magnetometry using a single-spin system in diamond, *Phys. Rev. B* **83**, 125410 (2011).
- [15] N. M. Nusran, M. U. Momeen, and M. V. G. Dutt, High-dynamic-range magnetometry with a single electronic spin in diamond, *Nat. Nanotechnol.* **7**, 109 (2012).
- [16] G. Waldherr, J. Beck, P. Neumann, R. S. Said, M. Nitsche, M. L. Markham, D. J. Twitchen, J. Twamley, F. Jelezko, and J. Wrachtrup, High-dynamic-range magnetometry with a single nuclear spin in diamond, *Nat. Nanotechnol.* **7**, 105 (2012).
- [17] C. Bonato, M. S. Blok, H. T. Dinani, D. W. Berry, M. L. Markham, D. J. Twitchen, and R. Hanson, Optimized quantum sensing with a single electron spin using real-time adaptive measurements, *Nat. Nanotechnol.* **11**, 247 (2016).
- [18] N. Wiebe and C. Granade, Efficient Bayesian Phase Estimation, *Phys. Rev. Lett.* **117**, 010503 (2016).
- [19] R. Santagati, A. A. Gentile, S. Knauer, S. Schmitt, S. Paesani, C. Granade, N. Wiebe, C. Osterkamp, L. P. McGuinness, J. Wang, M. G. Thompson, J. G. Rarity, F. Jelezko, and A. Laing, Magnetic-Field Learning Using a Single Electronic Spin in Diamond with One-Photon Readout at Room Temperature, *Phys. Rev. X* **9**, 021019 (2019).
- [20] E. Turner, S. H. Wu, X. Z. Li, and H. L. Wang, Real-time magnetometry with coherent population trapping in a nitrogen-vacancy center, *Phys. Rev. A* **105**, L010601 (2022).
- [21] J. K. Stockton, J. M. Geremia, A. C. Doherty, and H. Mabuchi, Robust quantum parameter estimation: Coherent magnetometry with feedback, *Phys. Rev. A* **69**, 032109 (2004).
- [22] N. Zhao, J. L. Hu, S. W. Ho, J. T. K. Wan, and R. B. Liu, Atomic-scale magnetometry of distant nuclear spin clusters via nitrogen-vacancy spin in diamond, *Nat. Nanotechnol.* **6**, 242 (2011).
- [23] M. D. Shulman, S. P. Harvey, J. M. Nichol, S. D. Bartlett, A. C. Doherty, V. Umansky, and A. Yacoby, Suppressing qubit dephasing using real-time Hamiltonian estimation, *Nat. Commun.* **5**, 5156 (2014).
- [24] C. Santori, P. Tamarat, P. Neumann, J. Wrachtrup, D. Fattal, R. G. Beausoleil, J. Rabeau, P. Olivero, A. D. Greentree, S. Prawer, F. Jelezko, and P. Hemmer, Coherent Population Trapping of Single Spins in Diamond Under Optical Excitation, *Phys. Rev. Lett.* **97**, 247401 (2006).
- [25] C. G. Yale, B. B. Buckley, D. J. Christle, G. Burkard, F. J. Heremans, L. C. Bassett, and D. D. Awschalom, All-optical control of a solid-state spin using coherent dark states, *Proc. Natl. Acad. Sci. USA* **110**, 7595 (2013).
- [26] D. A. Golter, T. Oo, M. Amezcua, I. Lekavicius, K. A. Stewart, and H. Wang, Coupling a Surface Acoustic Wave to an Electron Spin in Diamond via a Dark State, *Phys. Rev. X* **6**, 041060 (2016).
- [27] G. de Lange, Z. H. Wang, D. Riste, V. V. Dobrovitski, and R. Hanson, Universal dynamical decoupling of a single solid-state spin from a spin bath, *Science* **330**, 60 (2010).
- [28] W. Yang, W. L. Ma, and R. B. Liu, Quantum many-body theory for electron spin decoherence in nanoscale nuclear spin baths, *Rep. Prog. Phys.* **80**, 016001 (2017).
- [29] E. Togan, Y. Chu, A. Imamoglu, and M. D. Lukin, Laser cooling and real-time measurement of the nuclear spin environment of a solid-state qubit, *Nature (London)* **478**, 497 (2011).
- [30] H. Song, A. Chantasri, B. Tonekaboni, and H. M. Wiseman, Optimal mitigation of random-telegraph-noise dephasing by spectator-qubit sensing and control, [arXiv:2205.12567](https://arxiv.org/abs/2205.12567).